Effect of Second Phase Particle Size on the Recrystallized Microstructure of Mg–Al Alloys Following ECAE Processing

Chapter · January 2020

DOI: 10.1007/978-3-030-36647-6_27

CITATIONS
10

READS
131

7 authors, including:

Suhas Eswarappa Prameela
Johns Hopkins University
23 PUBLICATIONS **164** CITATIONS
SEE PROFILE

Peng Yi
Johns Hopkins University
43 PUBLICATIONS **608** CITATIONS
SEE PROFILE

Vance Liu
Micron Technology, Inc.
6 PUBLICATIONS **30** CITATIONS
SEE PROFILE

Beatriz Medeiros
Johns Hopkins University
2 PUBLICATIONS **25** CITATIONS
SEE PROFILE

Effect of Second Phase Particle Size on the Recrystallized Microstructure of Mg–Al Alloys Following ECAE Processing

Suhas Eswarappa Prameela, Peng Yi, Vance Liu, Beatriz Medeiros, Laszlo J. Kecskes, Michael L. Falk, and Timothy P. Weihs

Abstract

Magnesium (Mg) alloys are excellent candidates for structural applications, given their high strength to weight ratios. Grain boundaries and precipitates can both contribute to strengthening in Mg alloys, but the design of high strength Mg alloys is challenging due to Mg's anisotropic crystal lattice and yield asymmetry. Herein, we focus on thermomechanical processing that involves grain refinement in the presence of precipitates. We seek an understanding of how small and large $Mg_{17}Al_{12}$ intermetallic particles impact recrystallization and discontinuous precipitation in Mg–Al alloys. We do so by processing solution treated and peak aged Mg–9Al (wt%) alloys using equal channel angular extrusion (ECAE) along the Bc route at 150 °C. We find that the fine nanoprecipitates that nucleate within the solutionized grain interiors during ECAE processing lead to finer Mg grains in the recrystallized regions compared to those in the presence of the long lathlike precipitates produced during peak aging prior to ECAE processing.

Keywords

Deformation processing • Nanoprecipitates • Nucleation and growth • Recrystallization • Magnesium alloys

S. Eswarappa Prameela (✉) · P. Yi · V. Liu · B. Medeiros · M. L. Falk · T. P. Weihs
Department of Materials Science and Engineering, Johns Hopkins University, Baltimore, MD 21218, USA
e-mail: seswara3@jhu.edu

S. Eswarappa Prameela · P. Yi · L. J. Kecskes · M. L. Falk · T. P. Weihs
Hopkins Extreme Materials Institute, Johns Hopkins University, Baltimore, MD 21218, USA

M. L. Falk
Department of Mechanical Engineering, Johns Hopkins University, Baltimore, MD 21218, USA

Department of Physics and Astronomy, Johns Hopkins University, Baltimore, MD 21218, USA

Introduction

Robust and lightweight magnesium (Mg) alloys are desired in the automotive and defense industries, but the anisotropic behavior of Mg complicates our ability to control defect generation, texture development, and deformation behavior both during processing and in use. In particular, Mg's fundamental physical characteristics, including temperature-sensitive activation of different slip systems, strain rate sensitivities, and significant yield asymmetries, affect the selection of the most appropriate processing conditions [1–7]. Despite these limitations, we are gaining a better understanding of the underlying relationships related to the thermomechanical processing of Mg alloys, especially during severe plastic deformation (SPD). SPD techniques such as extrusion [8], rolling [9], or high-pressure torsion processing [10] have resulted in an extensive range of microstructures [4, 11]. A survey of these studies identifies specific challenges and opportunities in manipulating the microstructure of Mg and its alloys. One such instance is the possibility of creating fine grains with random texture, which improves strength and reduces the yield asymmetry. At the same time, continuous and discontinuous recrystallization processes have also been shown to enable grain refinement [12–14] and greater strengths. In certain alloy compositions, concurrent with recrystallization is the possible formation of fine precipitates [11, 13].

Precipitation is a phase transformation that involves nucleation and growth of second phase particles. There are three possible interactions between recrystallization and precipitation. First, both of these processes can occur simultaneously in different regions of a sample (e.g., precipitation in grain interior and recrystallization near grain boundary) during thermomechanical processing [13]. The second possibility is that recrystallization occurs alongside precipitation in the same region producing a combined reaction zone. The third instance is reprecipitation during recrystallization, wherein precipitates dissolve in the grains

J. B. Jordon et al. (eds.), *Magnesium Technology 2020*, The Minerals, Metals & Materials Series, https://doi.org/10.1007/978-3-030-36647-6_27

undergoing recrystallization and reform within or next to the new grains [15]. In this effort, we seek to gain a deeper understanding of the mechanisms that control this third mode of interaction in a Mg–9Al (wt%) binary alloy. Specifically, we study how the size of the precipitates within the grain interior can influence the overall recrystallization fraction and the final grain size in a combined reaction zone that includes recrystallized Mg grains and reprecipitated $Mg_{17}Al_{12}$ particles.

Experimental Procedure

We procured ingots of Mg–9Al (wt%) alloy from Magnesium Elektron North America (MENA), Madison, IL. The ingots were solutionized by heating them at 385 °C for 6 h and at 420 °C for 16 h, followed by a cold-water quench. Chemical analysis of the ingot was carried out using optical emission spectroscopy (OES) as shown in Table 1.

Two routes were followed for thermomechanical processing, as shown in Fig. 1. For Route 1, solution treated samples were deformed along the 4Bc route by equal channel angular extrusion (ECAE) at a rate of 0.15 mm/min at 150 °C with a 0.45 MPa backpressure. For Route 2, solution treated samples were first peak aged in a furnace for 163 h at 150 °C followed by ECAE along the 4Bc route with a rate of 0.15 mm/min at 150 °C with a 0.45 MPa backpressure. Samples were cut using a diamond wire saw after ECAE for light microscopy. We mechanically polished the sample using 800 and 1200 grit pads with water, followed by a cloth pad and OPS solution. Samples were then etched using a 2% Nital solution for characterization. Samples were also cut using a diamond wire saw for transmission electron microscopy (TEM). We then mechanically polished them to 50 µm slices and punched 3 mm disks. A Gatan precision ion polishing system (PIPS) was used to perforate holes with a thin region near the periphery for TEM observation. We employed a TF30 microscope operating at 300 keV for microstructure observations.

Results and Discussion

Light microscopy studies on samples after solution treatment and after peak aging confirm that there is no recrystallization before the ECAE processing. The grain size increases slightly during peak aging treatment in Route 2, but is deemed negligible. Thus, before the ECAE processing, both sets of samples have similar grains and grain sizes. The extrusion of the peak aged samples in Route 2, though, proved more challenging. As Fig. 2 indicates, shear localization, fracture, and profuse twinning occurred near the edge of the peak aged samples during ECAE. We attribute this occurrence to the existence of the long precipitate laths within the microstructure and the

Table 1 Primary constituents of the Mg–Al alloy as measured by optical emission spectroscopy

Chemical composition in weight percent (wt.%)										
Designation	Al	Cu	Mn	Zn	Ca	Ni	Be	Si	Fe	Mg
Mg–9Al (A9)	8.71	0.0002	0.005	<0.001	<0.001	0.0008	<0.0001	0.0020	0.0085	Balance

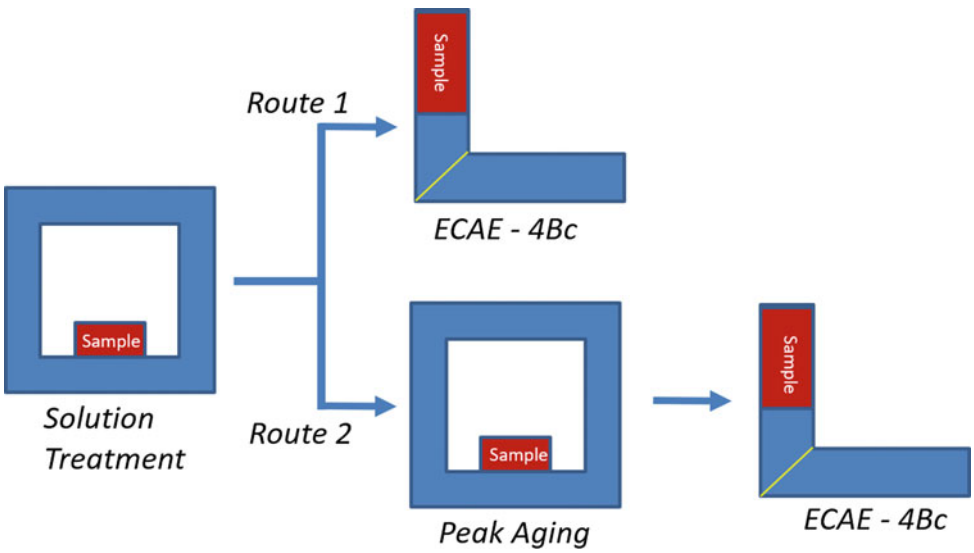

Fig. 1 Schematic of the two thermomechanical processing routes. Route 1: a solution treated A9 sample is processed via ECAE (4Bc) at 150 °C; Route 2: a solution treated sample is peak aged and then processed via ECAE (4Bc) at 150 °C

use of relatively low backpressure. Route 1 samples had no such issues, and all four extrusion passes were successful. Following four passes at 150 °C, light micrographs of samples from both processing routes (1 and 2) reveal river-like features in light micrographs, indicating that recrystallization begins along boundaries and grows into the grain interiors during extrusion (Fig. 3).

In our previous study [13], we describe and show that the recrystallized regions in Fig. 3a grow in volume as a function of ECAE passes of the Mg–9Al solutionized samples at 150 °C. A MATLAB code was used to analyze the area fraction of these regions after four passes for both Route 1 and Route 2. The recrystallized fraction for the Route 1 (A9 4Bc) sample is 57.7%, and it is 80.6% for the Route 2 (A9 peak aged + 4Bc) sample. Our earlier [13] and current TEM analysis (Figs. 4 and 5) reveal that the recrystallized regions are combined reaction zones containing recrystallized Mg grains and relatively small $Mg_{17}Al_{12}$ grains or precipitates sitting next to the Mg grains. The Mg grains contain near equilibrium concentrations of Al, as shown by HAADF-STEM and a random texture, as demonstrated by Kikuchi EBSD patterns [13].

The unrecrystallized portion of the microstructure also evolves during the ECAE processing in Route 1, and it is reported in detail in our earlier work [13]. At the end of the first pass, there are very few localized precipitates in the microstructure and some recrystallization near the grain boundary. After the second pass, the entire unrecrystallized region has a dense distribution of nanoprecipitates. The recrystallization region continues to grow as the number of passes increases, consuming the grain interior that contains finely spaced nanoprecipitates. At the start of the fourth pass, the microstructure still has a dense distribution of fine precipitates within the unrecrystallized grain interiors as shown in Fig. 4a, some of which will be recrystallized in the fourth and final pass. The nanoscale precipitates in the grain interiors of the Route 1 samples, with an almost spherical geometry and uniform distribution, stand in sharp contrast to the much larger, lathlike precipitates that result from peak-aging and are present in the grain interiors of the Route 2 samples prior to ECAE processing (Fig. 4c). (For completeness, we note that the precipitates are spaced more closely (discontinuous precipitates) near the grain boundary [16] in the Route 2 sample.)

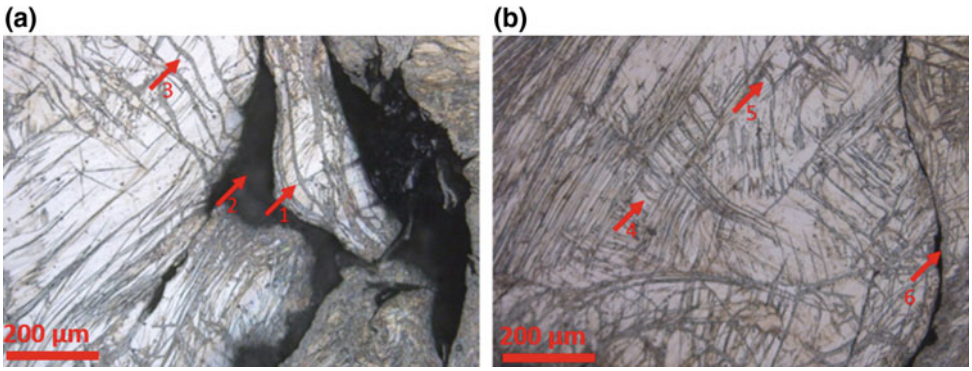

Fig. 2 **a**, **b** Bright field light micrographs showing recrystallization bands (arrows 1 and 3), extensive twinning (arrows 4 and 5) and fracture (arrows 2 and 6) close to the edge of Route 2 A9 peak aged + 4Bc sample

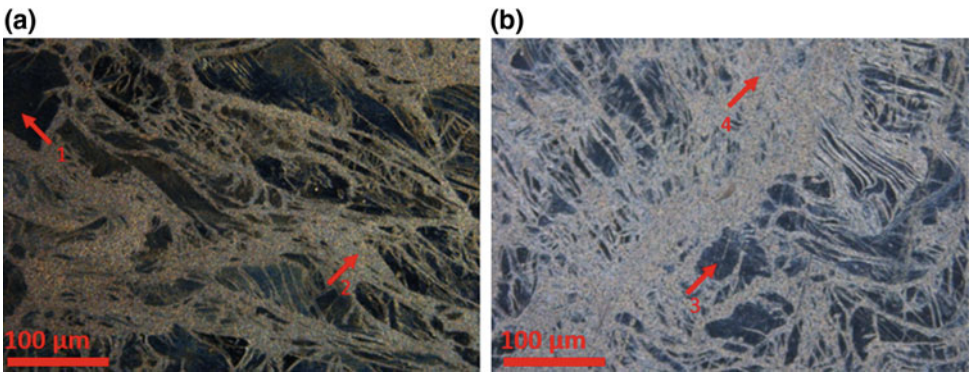

Fig. 3 Darkfield light micrographs showing **a** unrecrystallized region (arrow 1) and recrystallized region (arrow 2) in the Route 1 A9 4Bc sample; **b** unrecrystallized region (arrow 3) and recrystallized region (arrow 4) in the Route 2 A9 peak aged + 4Bc sample

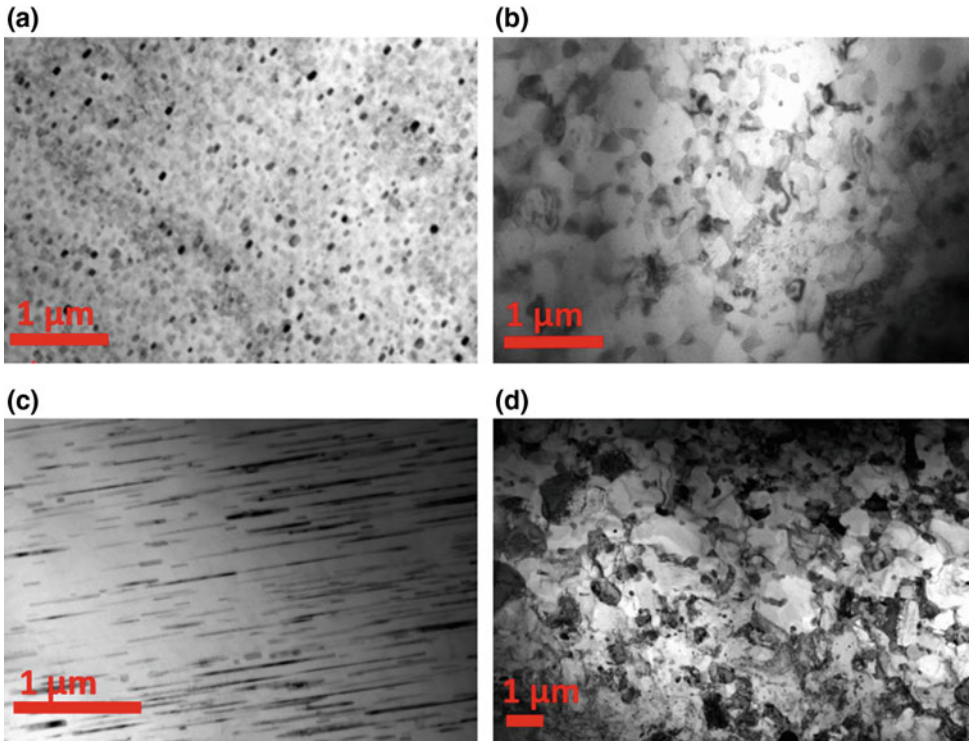

Fig. 4 TEM micrographs showing **a** a dense distribution of $Mg_{17}Al_{12}$ nanoprecipitates in the grain interior of the Route 1 A9 4Bc sample; **b** a combined reaction zone near a grain boundary in the Route 1 A9 4Bc sample; **c** a coarse distribution of Route 2 $Mg_{17}Al_{12}$ laths in the grain interior of the A9 peak aged + 4Bc sample; and **d** a combined reaction zone near a grain boundary in the Route 2 A9 peak aged + 4Bc sample (*Note* that '4' here refers to the number of ECAE passes)

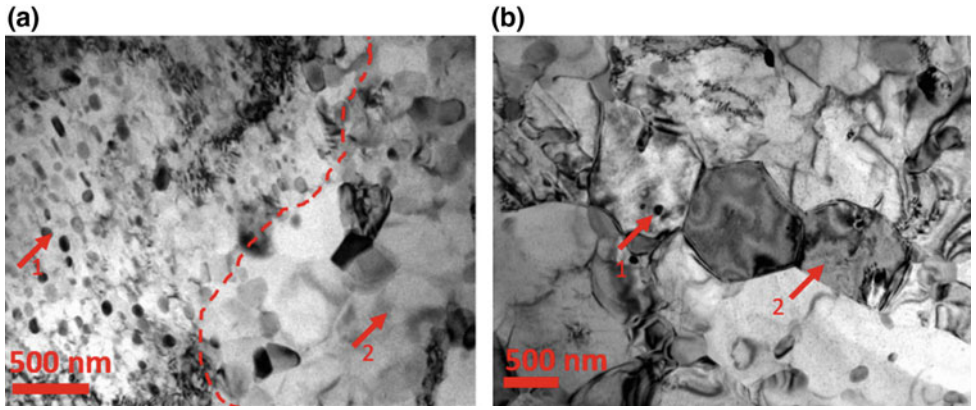

Fig. 5 **a** Fine nanoprecipitates on the left (arrow 1) intersecting with the advancing combined reaction zone (arrow 2) in the A9 4Bc (Route 1) sample. The growth front of the combined reaction is shown by the dashed line; **b** fine $Mg_{17}Al_{12}$ particle (arrow 1) within a large grain (similar to another Mg grain exemplified by arrow 2) in the combined reaction zone, as seen in the peak aged + A9 4Bc (Route 2) sample

In Fig. 4b, d, we show the recrystallized microstructures within the combined reaction zones for the Route 1 and 2 samples, respectively, that grow in volume with each ECAE pass. The TEM images reveal much finer Mg grain sizes in the Route 1 combined reaction zones compared to Route 2, and Fig. 6 shows a statistical analysis of these grain sizes.

Higher-resolution TEM images in Fig. 5 begin to reveal the interaction between recrystallization and precipitates. In Fig. 5a, a red dashed line marks the boundary between an original ~250 μm Mg grain and a recrystallized region for Route 1. We see fine precipitate particles within the original grain on the left side of the dashed red boundary. These precipitate particles form via continuous precipitation in the

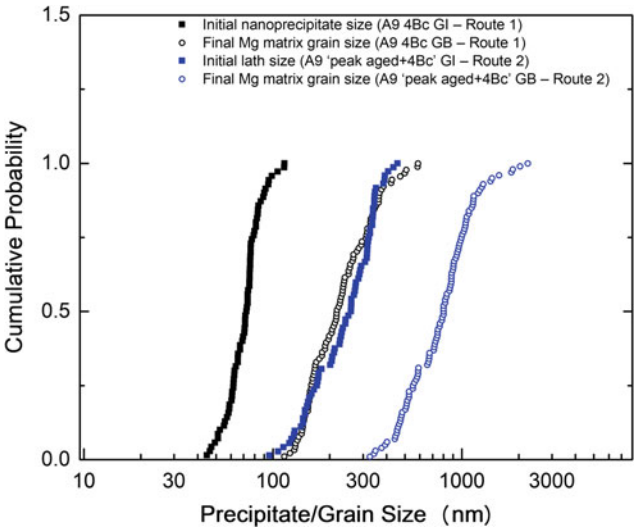

Fig. 6 Cumulative density plots of the sizes of the initial $Mg_{17}Al_{12}$ particle within grain interiors and the final recrystallized Mg matrix grains of the samples processed along Routes 1 and 2

original grain during the first two ECAE passes [13]. On the right side of the dashed red boundary, we see the combined reaction zone in the recrystallized region that contains small, precipitate-free Mg grains and larger $Mg_{17}Al_{12}$ particles at the boundaries of the Mg grains. In the Route 2 sample, we did not capture a boundary between the unrecrystallized and recrystallized regions, in part due to the higher level of recrystallization in Route 2 samples. However, Fig. 5b reveals the microstructure in a recrystallized region after Route 2 processing. The $Mg_{17}Al_{12}$ laths that initially resided in the grain interiors are absent, and as in Route 1, the resulting Mg grains are also much smaller than the larger (~250 μm), initial Mg grains. The recrystallization consumes the whole volume in Fig. 5b, and in contrast to the resulting Route 1 microstructure, the resulting Route 2 combined reaction zone shows that small $Mg_{17}Al_{12}$ particles have reprecipitated both within and outside the new, small Mg grains.

To quantify differences in the microstructures for the two processing routes, we show a statistical analysis of the initial $Mg_{17}Al_{12}$ precipitates in the grain interiors (Fig. 4a, c) and the final, recrystallized Mg grains (Fig. 4b, d) in the combined reaction zones for Routes 1 and 2 in Fig. 6. This figure reveals that the finer initial precipitates in Route 1 correlate with finer Mg grain sizes in the combined reaction zone while the larger initial precipitates (laths) in Route 2 correlate with larger Mg grains in the combined reaction zone.

Based on these results, we can state correlations that can be contrasted for Routes 1 and 2. The initial nanoscale $Mg_{17}Al_{12}$ precipitates (72.31 nm average) that exist before and during recrystallization in Route 1 correlate with less recrystallization (57.7%), a finer average recrystallized Mg grain size (245.22 nm average), and a coarser reprecipitated $Mg_{17}Al_{12}$ particle size (216.85 nm average, measured from Fig. 4b) compared to Route 2. In contrast, the much larger, lathlike $Mg_{17}Al_{12}$ precipitates (252.7 nm average) that exist at the start of ECAE processing in Route 2 correlate with a higher area fraction of recrystallization (80.6%), a larger average recrystallized Mg grain size (838.69 nm average), and a finer reprecipitated $Mg_{17}Al_{12}$ particle size (86.99 nm average, measured from Fig. 4d) compared to Route 1.

The difference in the recrystallized microstructures between the two routes is likely a result of the interaction between the precipitates and the recrystallization processes. The presence of precipitate particles before recrystallization could affect the nucleation and growth of the recrystallized grain [17]. Conversely, the kinetics of recrystallization could affect reprecipitation within the combined reaction zone.

We first consider the potential effect of the initial precipitates on the nucleation of new Mg grains, and the process called particle stimulated nucleation (PSN). When the precipitates are sufficiently large, they can stimulate the nucleation of new grains. The critical particle radius for PSN is given by $r^* = 4\gamma/0.5\rho G b^2$ where γ is the grain boundary free energy, ρ is the dislocation density, G is the shear modulus, b is the Burgers vector. Using 0.5 J/m^2 for γ, 10^{14} m^{-2} for ρ, 18 GPa for G, and 3.2 Å for b, we obtain $r^* \sim 20$ μm. Robson et al. also reported a critical PSN radius greater than 1 μm [18]. Given both the predicted and reported critical radii are larger than those measured for the initial particles in Route 1 and Route 2, we expect that PSN is inactive for both sets of samples. Instead of PSN, we anticipate that recrystallization is initiated from highly strained areas near grain boundaries, consistent with our observations and previous studies [13].

Based on Fig. 6, the average recrystallized Mg grain size for Route 2 (838.69 nm) is about 3.4 times the average recrystallized Mg grain size for Route 1 (245.22 nm). Given that the recrystallization area fraction for Route 2 (80.6%) is only 1.4 times larger than for Route 1 (57.7%), we estimate that the number of recrystallized grains for Route 2 must be 6 times lower than for Route 1. We explain this disparity by considering differences in the rates of nucleation of new Mg grains or differences in the growth of these Mg grains. In an earlier study [13], we considered the impact of solute content in unrecrystallized regions of Route 1 samples and its ability to promote nucleation of new Mg grains. Here, we focus on growth and assume that new Mg grains nucleate at a similar rate in both processing routes. Thus, the grains in Route 2 must be growing more rapidly than in Route 1. To seek an explanation for this hypothesis, we considering the pinning effects of the initial $Mg_{17}Al_{12}$ particles.

It is well established that the Zener pinning effect of dense and small second phase particles prevents the growth of recrystallized grains. For example, Fig. 5a shows dense

and fine particles near the growth front of the recrystallized grain, and that could pin the growth front in the Route 1 sample. The critical grain size for continuing growth is $d^* = 4\gamma/\left(0.5\rho Gb^2 - \frac{3F_v\gamma}{r}\right)$, where F_v is the volume fraction of the second phase (precipitate), and r is the second phase particle radius. This formula is derived for a spherical second phase particle, where F_v/r is also proportional to the inverse of the particle spacing, i.e., L^{-1}. Given the average particle radius and spacing (L) is much smaller for Route 1 [19], d^* is larger, and the recrystallized Mg grains are more likely to be pinned in Route 1 than in Route 2, once they nucleate. If the growth of recrystallized grains is hindered by the high density of fine precipitate particles in Route 1 processing, more grains must nucleate to consume the heavily deformed grains. In contrast, we argue that grain growth is less impeded and easier during Route 2 due to limited Zener pinning via the larger $Mg_{17}Al_{12}$ particles. Once nucleated, the Mg grains can grow to a larger average size, and thus less nucleation of new Mg grains is required to recrystallize most of the sample volume.

As a final observation, we note that the boundaries of the recrystallized grains can serve as channels for solute transport within the combined reaction zone. Due to the finer recrystallized Mg grain size of the Route 1 samples, there are more grain boundaries. In turn, this enables a more rapid and efficient transport of Al, which allows more extensive coarsening of the $Mg_{17}Al_{12}$ particles that have reprecipitated. This could explain why the average size of the reprecipitated particles following Route 1 processing is 216.85 nm, and it is only 86.99 nm following Route 2 processing. This difference in particle size also correlates with the much lower solute concentration in the recrystallized region in Route 1 compared to Route 2. The finer recrystallized Mg grain size of the Route 1 samples thus appears to be enabling a more rapid depletion of Al from the Mg matrix and a more extensive coarsening of the $Mg_{17}Al_{12}$ particles.

Conclusions

A binary Mg–Al alloy was used to study the effect of precipitate size and morphology on the evolution of the combined reaction zone and resulting grain sizes. Smaller $Mg_{17}Al_{12}$ particles produced during the ECAE process appear to produce a strong pinning effect and are likely inhibiting the growth of recrystallized Mg grains. In contrast, large precipitate laths produced during peak aging before ECAE processing appear to promote recrystallization by enabling more extensive growth of the recrystallized Mg grains. In addition, the finer resulting Mg grain size in Route 1 processing may promote the coarsening of the reprecipitated $Mg_{17}Al_{12}$ particles via more extensive grain boundary diffusion compared to Route 2 samples. The step by step process by which fine particles or large laths dissolve and help in forming the combined reaction zone is still not clear. The competition between the dissolution rate of prior precipitates or laths and the nucleation rate of the new precipitates may play an essential role during this process, and an improved understanding of the interplay of precipitation, reprecipitation, growth, and recrystallization is needed.

Acknowledgements The authors would like to gratefully acknowledge the financial and technical support from the Center for Materials under Extreme Dynamic Environment (CMEDE). The research was sponsored by the Army Research Laboratory and was accomplished under Cooperative Agreement Number W911NF-12-2-0022. The views and conclusions contained in this document are those of the authors and should not be interpreted as representing the official policies, either expressed or implied, of the Army Research Laboratory or the US Government. The US Government is authorized to reproduce and distribute reprints for Government purposes notwithstanding any copyright notation herein.

References

1. J. Robson, Anisotropy and Asymmetry of Yield in Magnesium Alloys at Room Temperature, Metall. Mater. Trans. A. 45 (2014) 5226–5235. https://doi.org/10.1007/s11661-014-2453-4.
2. J.D. Robson, N. Stanford, M.R. Barnett, Effect of particles in promoting twin nucleation in a Mg–5wt.% Zn alloy, Scr. Mater. 63 (2010) 823–826. https://doi.org/10.1016/j.scriptamat.2010.06.026.
3. S. Bagherzadeh, K. Abrinia, Y. Liu, Q. Han, The effect of combining high-intensity ultrasonic vibration with ECAP process on the process parameters and mechanical properties and microstructure of aluminum 1050, Int. J. Adv. Manuf. Technol. 88 (2016). https://doi.org/10.1007/s00170-016-8779-x.
4. Z. Wu, R. Ahmad, B. Yin, S. Sandlöbes, W.A. Curtin, Mechanistic origin and prediction of enhanced ductility in magnesium alloys, Science. 359 (2018) 447–452. https://doi.org/10.1126/science.aap8716.
5. D. Mallick, S. Eswarappa Prameela, V. Kannan, M. Zhao, J. Lyod, T.P. Weihs, K.T. Ramesh, On the Role of Texture and Precipitate Orientation in Spall Failure of a Rolled Magnesium Alloy, in Bull. Am. Phys. Soc. 64(8) (2019). http://meetings.aps.org/Meeting/SHOCK19/Session/1C.2.
6. X. Ma, S., Eswarappa-Prameela, N. Krywopusk, L.J. Kecskes, T. Sano, T. P. Weihs, Dynamic precipitation in a binary Mg-Al Alloy during Equal Channel Angular Extrusion (ECAE). Microsc. Microanal. 24(S1) (2018) 2222–2223.
7. S. Eswarappa Prameela, T.P. Weihs, Deformation Driven Precipitation in Binary Magnesium Alloys. Magnes. Technol. (2020). https://doi.org/10.1007/978-3-030-36647-6_26
8. V.M. Segal, Engineering and commercialization of equal channel angular extrusion (ECAE), Mater. Sci. Eng. A. 386 (2004) 269–276. https://doi.org/10.1016/j.msea.2004.07.023.
9. T.-C. Chang, J.-Y. Wang, C.-M. O, S. Lee, Grain refining of magnesium alloy AZ31 by rolling, J. Mater. Process. Technol.

140 (2003) 588–591. https://doi.org/10.1016/s0924-0136(03)00797-0.
10. A.S.J. Al-Zubaydi, A.P. Zhilyaev, S.C. Wang, P. Kucita, P.A.S. Reed, Evolution of microstructure in AZ91 alloy processed by high-pressure torsion, J. Mater. Sci. 51 (2016) 3380–3389. https://doi.org/10.1007/s10853-015-9652-2.
11. J.-F. Nie, Precipitation and Hardening in Magnesium Alloys, Metall. Mater. Trans. A. 43 (2012) 3891–3939. https://doi.org/10.1007/s11661-012-1217-2.
12. R. Cottam, J. Robson, G. Lorimer, B. Davis, Dynamic recrystallization of Mg and Mg–Y alloys: Crystallographic texture development, Mater. Sci. Eng. A. 485 (2008) 375–382. https://doi.org/10.1016/j.msea.2007.08.016.
13. X.L. Ma, S. Eswarappa Prameela, P. Yi, M. Fernandez, N.M. Krywopusk, L.J. Kecskes, T. Sano, M.L. Falk, T.P. Weihs, Dynamic precipitation and recrystallization in Mg-9wt.%Al during equal-channel angular extrusion: A comparative study to conventional aging, Acta Mater. 172 (2019) 185–199. https://doi.org/10.1016/j.actamat.2019.04.046.
14. Z.R. Zeng, Y.M. Zhu, S.W. Xu, M.Z. Bian, C.H.J. Davies, N. Birbilis, J.F. Nie, Texture evolution during static recrystallization of cold-rolled magnesium alloys, Acta Mater. 105 (2016) 479–494. https://doi.org/10.1016/j.actamat.2015.12.045.
15. S.-H. Kim, J.U. Lee, Y.J. Kim, B.G. Moon, B.S. You, H.S. Kim, S.H. Park, Improvement in extrudability and mechanical properties of AZ91 alloy through extrusion with artificial cooling, Mater. Sci. Eng. A. 703 (2017) 1–8. https://doi.org/10.1016/j.msea.2017.07.048.
16. J.B. Clark, Age hardening in a Mg-9 wt.% Al alloy, Acta Metall. 16 (1968) 141–152. https://doi.org/10.1016/0001-6160(68)90109-0.
17. F.J. Humphreys, M. Hatherly, Chapter 9 - Recrystallization of Two-Phase Alloys, in: F.J. Humphreys, M. Hatherly (Eds.), Recryst. Relat. Annealing Phenom. Second Ed., Elsevier, Oxford, 2004: pp. 285–319. https://doi.org/10.1016/b978-008044164-1/50013-x.
18. J.D. Robson, D.T. Henry, B. Davis, Particle effects on recrystallization in magnesium–manganese alloys: Particle-stimulated nucleation, Acta Mater. 57 (2009) 2739–2747. https://doi.org/10.1016/j.actamat.2009.02.032.
19. S. Eswarappa Prameela, P. Yi, B. Medeiros, V. Liu, J.K. Laszlo, M.L. Falk, T.P. Weihs, Deformation assisted nucleation of continuous nanoprecipitates in Mg-Al Alloys (Nov 11 2019). Available at SSRN: https://ssrn.com/abstract=3484667.